Photoproduction of spin and charge carriers in halogen-bridged binuclear platinum chain complexes

2008 J. Phys.: Condens. Matter 20 415215

(http://iopscience.iop.org/0953-8984/20/41/415215)

J. Phys.: Condens. Matter **20** (2008) 415215 (9pp) doi:10.1088/0953-8984/20/41/415215

Photoproduction of spin and charge carriers in halogen-bridged binuclear platinum chain complexes

Shoji Yamamoto and Jun Ohara

Department of Physics, Hokkaido University, Sapporo 060-0810, Japan

Received 21 June 2008, in final form 30 August 2008
Published 18 September 2008
Online at stacks.iop.org/JPhysCM/20/415215

Abstract

Nonlinear lattice relaxation of photoexcited diplatinum-halide chain compounds is theoretically investigated within a one-dimensional extended Peierls–Hubbard model. We first illuminate the whole relaxation scenario in terms of variational wavefunctions and then visualize each relaxation channel numerically integrating the Schrödinger equation. High-energy excitations above the electron–hole continuum tend to relax into polarons, while excitons pumped within the optical gap, unless luminescent, turn into solitonic states nonradiatively. Neutral and charged solitons coexist as stable photoproducts, which has never been observed in conventional platinum-halide chains, and they are highly resonant on the occasion of their birth and geminate recombination.

(Some figures in this article are in colour only in the electronic version)

1. Introduction

Halogen (X)-bridged binuclear transition-metal (M) linear-chain complexes [1–4] have stimulated a renewed interest in the MX class of materials [5, 6]. Metal binucleation induces an unpaired electron per metal-dimer unit even in valence-trapped states, contrasting with the Peierls-gapped state of M^{2+} and M^{4+} in conventional MX chains. The Md_{z^2}–Md_{z^2} direct overlap effectively reduces the on-site Coulomb repulsion due to its d_{σ^*} character, remarkably enhancing the electron itinerancy. The MMX electronic state is thus activated and full of variety [7, 8]. Diplatinum-halide varieties, $A_4[Pt_2(pop)_4X]\cdot mH_2O$ (X = Cl, Br, I; A = NH_4, Na, K, ...; pop = diphosphonate = $P_2O_5H_2$) [1, 2] structurally resemble conventional MX compounds and exhibit the most likely charge density wave (CDW) with the halogen-sublattice dimerized [9, 10]: $-X^- \cdots Pt^{2+}Pt^{2+} \cdots X^- - Pt^{3+}Pt^{3+} - X^- \cdots$. However, the ground state is quite sensitive to bridging halogens and counter ions [11, 12]. In the iodo complexes the valence arrangement is highly tunable with pressure application and optical irradiation [13–18]. Their analogue without any counter ion, $Pt_2(dta)_4I$ (dta = dithioacetate = CH_3CS_2) [3], is of metallic conduction above room temperature [19, 20]. With decreasing temperature, it undergoes successive phase transitions [21–24] and ends up with a distinct Peierls-distorted state of alternating charge polarization (ACP) [25, 26]: $\cdots I^- \cdots Pt^{2+}Pt^{3+} - I^- - Pt^{3+}Pt^{2+} \cdots I^- \cdots$, where the metal sublattice, which is free from any hydrogen bonding, is dimerized. The methyl group in the dta ligand can be replaced by longer alkyl chains [27, 28] so as to enhance the one-dimensionality.

Photoexcited MX complexes are more and more interesting. By analogy with topological excitations in the trans-isomer of polyacetylene, several authors [29–31] had an idea of various defect states existing in PtX chains. Solitonic and polaronic excitations [5, 6, 32–34] were particularly investigated in relation to experimental findings. Such charge and/or spin carriers may be less massive and more mobile in Pt_2X chains with much smaller bandgaps [35, 36]. There indeed appear new vibrational features in the resonant Raman spectra of $K_4[Pt_2(pop)_4Cl]\cdot H_2O$, which can be ascribed to polaronic defects due to the deficiency of counter ions [37]. Electron-spin-resonance (ESR) measurements on $Pt_2(C_5H_{11}CS_2)_4I$ reveal thermally activated mobile spins attributable to neutral solitons [38]. Photoexcitation is a promising approach to producing these valence anomalies in a systematic fashion. Thus motivated, we analyse the electron–lattice dynamics of photoexcited Pt_2X chains. We first reveal the whole relaxation scenario in terms of variational wavefunctions and then visualize each story as a solution of the Schrödinger equation. Neutral solitons and/or polarons were observed in $[Pt(en)_2Cl](ClO_4)_2$ (en = ethylenediamine =

$C_2H_8N_2$) [39–41], whereas charged solitons and polarons were in $[Pt(en)_2I](ClO_4)_2$ [42, 43]. However, neutral and charged solitons do not seem able to coexist as photoproducts in any MX chain [32, 44]. There may be a wider variety of relaxation channels in varied MMX chains [45].

2. Modelling

We describe Pt_2X chains by the $\frac{3}{4}$-filled single-band Peierls–Hubbard Hamiltonian

$$\begin{aligned}\mathcal{H} = &-\sum_{n,s}\left[t_{\mathrm{MXM}} - \alpha(l_{n+1}+r_n)\right]\left(a^{\dagger}_{n+1,s}b_{n,s} + b^{\dagger}_{n,s}a_{n+1,s}\right)\\ &- t_{\mathrm{MM}}\sum_{n,s}\left(b^{\dagger}_{n,s}a_{n,s} + a^{\dagger}_{n,s}b_{n,s}\right)\\ &- \beta\sum_{n,s}(l_n n_{n,s} + r_n m_{n,s}) + \frac{K_{\mathrm{MX}}}{2}\sum_n\left(l_n^2 + r_n^2\right)\\ &+ \frac{M_{\mathrm{X}}}{2}\sum_n \dot{u}_n^2 + M_{\mathrm{M}}\sum_n \dot{v}_n^2\\ &+ U_{\mathrm{M}}\sum_n(n_{n,\uparrow}n_{n,\downarrow} + m_{n,\uparrow}m_{n,\downarrow})\\ &+ \sum_{n,s,s'}(V_{\mathrm{MM}}n_{n,s}m_{n,s'} + V_{\mathrm{MXM}}n_{n+1,s}m_{n,s'}),\end{aligned} \tag{2.1}$$

where $n_{n,s} = a^{\dagger}_{n,s}a_{n,s}$ and $m_{n,s} = b^{\dagger}_{n,s}b_{n,s}$ with $a^{\dagger}_{n,s}$ and $b^{\dagger}_{n,s}$ creating an electron with spin $s = \uparrow, \downarrow \equiv \pm$ on the Ptd_{z^2} orbitals in the nth diplatinum unit. t_{MM} and t_{MXM} describe the intradimer electron transfer and the interdimer electron supertransfer, respectively, and are set for $t_{\mathrm{MM}} = 2t_{\mathrm{MXM}}$. α and β characterize electron–lattice interactions of the Peierls and Holstein types, respectively. $l_n = v_n - u_{n-1}$ and $r_n = u_n - v_n$, with u_n and v_n being, respectively, the chain-direction displacements of the nth halogen ion and diplatinum cluster from their equilibrium positions. Deformation of every diplatinum cluster is negligible. K_{MX} is the platinum–halogen spring constant, while M_{X} and $2M_{\mathrm{M}}$ are the masses of a halogen atom and a diplatinum complex, respectively. Any calculation is carried out in a chain of a hundred or more Pt_2X units under the periodic boundary condition, where no significant size effect survives.

We show in figure 1 a ground-state phase diagram of the Hamiltonian (2.1) within the Hartree–Fock (HF) approximation. The site-diagonal Holstein-type electron–lattice coupling stabilizes the CDW state against the Mott–Hubbard (MH) insulating state, while the site-off-diagonal Peierls-type one contributes towards realizing the ACP state. We consider both pop and dta families of Pt_2X complexes, setting $(\alpha, \beta)/\sqrt{t_{\mathrm{MXM}}K_{\mathrm{MX}}}$ equal to $(0.0, 1.2)$ and $(0.3, 0.8)$, respectively. Typical PtX chains lie in the intermediate-correlation regime [6, 32] of $V_{\mathrm{MXM}} \ll U_{\mathrm{M}} \lesssim t_{\mathrm{MXM}}$ and platinum binucleation should effectively reduce the on-site repulsion. Thus we fix the Pt_2X Coulomb parameters at $(U_{\mathrm{M}}, V_{\mathrm{MM}}, V_{\mathrm{MXM}})/t_{\mathrm{MXM}} = (0.5, 0.25, 0.15)$. The d–p hybridization and the resultant interdimer supertransfer significantly depend on the bridging halogens. The Pt–I transfer integral is indeed a few times as large as the Pt–Cl one [37, 46]. The present parametrization well features Pt_2X chains, but the Coulomb parameters, when scaled, may fundamentally vary with X.

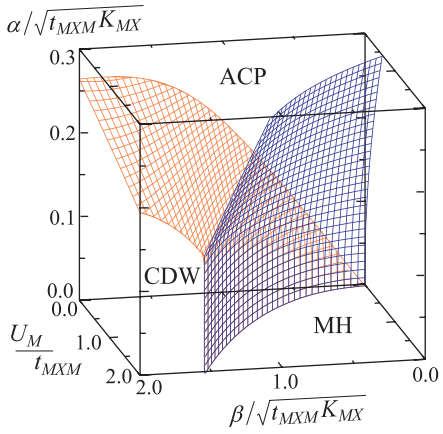

Figure 1. Hartree–Fock calculation of a ground-state phase diagram on the α-β-U_{M} cube for MMX chains.

3. Variational calculation

Photoinduced charge-transfer excitations first spread over the chain and then transform themselves into local defects. Such self-localization processes can be visualized through the calculation of adiabatic potential energy surfaces in a variational manner [32, 33, 44, 45]. Solitonic relaxation channels are describable with a trial wavefunction

$$\begin{aligned} l_n &= \sigma(-1)^n\lambda\left[1 + \kappa\left(\tanh\frac{|n| - d/2}{\xi} - 1\right)\right],\\ r_n &= (-1)^n\lambda\left[1 + \kappa\left(\tanh\frac{|n+\delta| - d/2}{\xi} - 1\right)\right],\end{aligned} \tag{3.1}$$

whereas polaronic ones with

$$\begin{aligned} l_n &= \sigma(-1)^n\lambda\left[1 + \kappa\left(\tanh\left|\frac{|n| - d/2}{\xi}\right| - 1\right)\right],\\ r_n &= (-1)^n\lambda\left[1 + \kappa\left(\tanh\left|\frac{|n+\delta| - d/2}{\xi}\right| - 1\right)\right],\end{aligned} \tag{3.2}$$

where the variational parameters κ, ξ and δ are determined at every interdefect distance d given so as to minimize the energy of the lowest-lying excited state, setting λ equal to the uniform halogen-ion displacement relative to neighbouring diplatinum clusters in the CDW ($\sigma = 1$) or ACP ($\sigma = -1$) ground state. Once the ground state is photoexcited into the Frank–Condon state, which still sits at $\kappa = 0$, the uniform bond alternation begins to be locally deformed. Increasing κ with d remaining to be zero depicts the self-stabilization of a charge-transfer exciton. The fully stabilized, that is to say, self-trapped exciton (STE) may have paths to a pair of solitons and antisolitons and that of polarons. Such defect pairs may be directly generated from free electron–hole pairs, which are higher-lying excited states, with κ and d being tuned simultaneously. ξ determines the width of a defect. δ is just a minor parameter, bringing the defect centre any other types of valence oscillation besides the ground-state one [36].

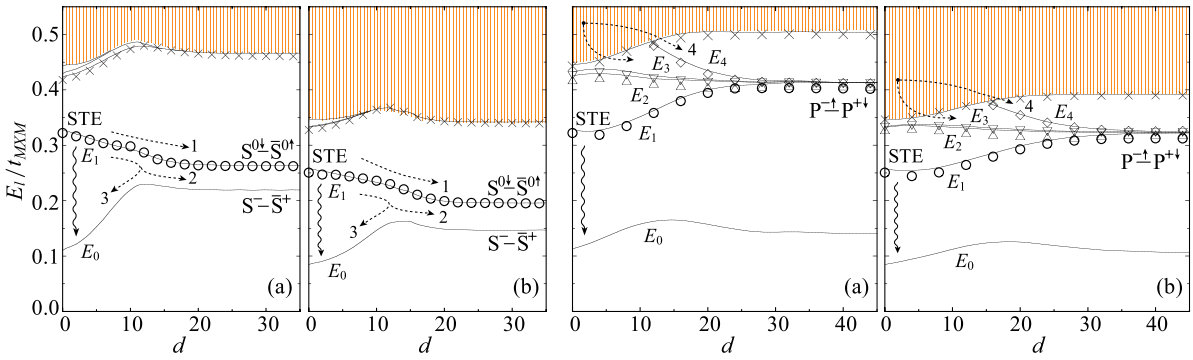

Figure 2. The solitonic (the left two panels) and polaronic (the right two panels) relaxation channels of photoexcited Pt_2X chains whose ground states are of the CDW (a) and ACP (b) types, which are relevant to $A_4[Pt_2(pop)_4X]\cdot mH_2O$ and $Pt_2(dta)_4I$, respectively. $E_l^{\rm HF}$ is plotted by solid lines, while $E_l^{\rm CI}$ by symbols. A fully stabilized exciton, unless it decays by luminescence, may be dissociated into a neutral (1) or charged (2) soliton (S)–antisoliton ($\bar{S}$) pair. Any potential soliton pair is so fragile as to recombine and disappear (3). Polaron (P) pairs may be generated by high-energy excitations reaching the electron–hole continuum.

The lattice configuration is adiabatically determined within the HF scheme. The ground-state bond-alternation amplitude λ minimizes $\langle E_0|\mathcal{H}|E_0\rangle \equiv E_0$ in a chain of constant length, where

$$|E_0\rangle = \prod_{\epsilon_{\mu,s}\leqslant\epsilon_{\rm F}} c^\dagger_{\mu,\uparrow}c^\dagger_{\mu,\downarrow}|0\rangle, \tag{3.3}$$

with $|0\rangle$ denoting the true electron vacuum, $\epsilon_{\rm F}$ indicating the Fermi energy and $c^\dagger_{\mu,s}$, generally given as $\sum_n(\vartheta_{\mu,n,s}a^\dagger_{n,s} + \varphi_{\mu,n,s}b^\dagger_{n,s})$, creating an electron of spin s in the HF eigenstate of eigenvalue $\epsilon_{\mu,s}$. The excited-state parameters κ, ξ and δ minimize ${}_{\rm HF}\langle E_1|\mathcal{H}|E_1\rangle_{\rm HF}$, where

$$|E_l\rangle_{\rm HF} = c^\dagger_{\nu,s}c_{\mu,s}|E_0\rangle, \tag{3.4}$$

provided $\epsilon_{\mu,s} \leqslant \epsilon_{\rm F} < \epsilon_{\nu,s}$. For the first excited state $l = 1$, μ and ν are set equal to the highest-lying occupied and lowest-lying vacant levels, respectively. When we take particular interest in the lth energy surface, ${}_{\rm HF}\langle E_l|\mathcal{H}|E_l\rangle_{\rm HF}$ may be minimized instead. However, the whole energy scheme is not so sensitive to the variational target as to be qualitatively changeable. In any case the HF lth excited-state energy $E_l^{\rm HF}$ is trivially written as $E_0 + \epsilon_{\nu,s} - \epsilon_{\mu,s}$.

We further consider configuration interactions (CIs) between the HF excited states in an attempt to describe Coulomb correlations with more precision. Excited states of the single-particle–hole CI type are expressed as

$$|E_l\rangle_{\rm CI} = \sum_{\epsilon_{\mu,s}\leqslant\epsilon_{\rm F}<\epsilon_{\nu,s}} f(\mu,\nu,s;l)c^\dagger_{\nu,s}c_{\mu,s}|E_0\rangle, \tag{3.5}$$

where $f(\mu,\nu,s;l)$ diagonalizes the original Hamiltonian (2.1). The refined lth excited-state energy $E_l^{\rm CI}$ is given by ${}_{\rm CI}\langle E_l|\mathcal{H}|E_l\rangle_{\rm CI}$.

Figure 2 presents the thus-calculated adiabatic potential energies as functions of d, where the ground-state energy is set to zero. Even though fully stabilized excitons are most likely to decay directly into the ground state, whether radiatively or nonradiatively, we take particular interest in their relaxing further into solitonic states. No energy barrier between an STE and any S–$\bar{S}$ pair, which is not the case with PtX chains [32, 44], allows STEs to decay rather fast. Solitons have localized wavefunctions and their overlap rapidly decreases with increasing d. Instantaneous charge transport between far distant S and $\bar{S}$ is hardly feasible. Therefore, tunnelling between the energy surfaces E_1 and E_0 occurs at a moderate separation. Charged soliton pairs may be less reachable than neutral ones, because assistant lattice fluctuations of odd parity [44] are necessary to their occurrence. In any case, once a pair of solitons and antisolitons is generated at a certain distance, say, $d \gtrsim 20$, they must be long-lived owing to an energy barrier to the ground state, especially on an ACP background. On the other hand, there is no possibility of an STE changing into a polaron pair. Polaronic states are available from the electrons pumped above the optical gap. Polaron pairs disappear into STEs, which are either luminescent or ready for further relaxation into solitonic states (see figures 5 and 6 later on).

Indeed there are Coulomb-correlation-induced configuration interactions, especially in the small-d region, but the correction $E_l^{\rm CI} - E_l^{\rm HF}$ is not so significant in Pt_2X chains of moderate Coulomb correlations. It is not the case with Ni_2I chains of $U_{\rm M} \gg t_{\rm MXM}$ [47]. Since the most important variational prediction of neutral and charged solitons coexisting as stable photoproducts remains unchanged with the CI refinement of the energy surfaces, we reasonably employ the time-dependent HF method in order to verify this scenario.

4. Real-time dynamics

We trace charge-transfer excitations as functions of real time solving of the Schrödinger equation:

$$\mathrm{i}\hbar\dot{\Psi}_{\mu,s}(t) = \mathcal{H}_s^{\rm HF}(t)\Psi_{\mu,s}(t), \tag{4.1}$$

where $\mathcal{H}_s^{\rm HF}(t)$ and $\Psi_{\mu,s}(t)$, the spin-s sectors of the HF Hamiltonian and wavefunction, are given by a square matrix and a column vector of degree $2N$, respectively. Defining the

wavevector as

$$\Psi_{\mu,s}(t) = \begin{bmatrix} \vartheta_{\mu,1,s}(t) \\ \varphi_{\mu,1,s}(t) \\ \vdots \\ \vartheta_{\mu,N,s}(t) \\ \varphi_{\mu,N,s}(t) \end{bmatrix}, \tag{4.2}$$

and employing a unitary transformation

$$U = \begin{bmatrix} 0 & 1 & 0 & \cdots & 0 \\ 0 & 0 & 1 & \ddots & \vdots \\ \vdots & \ddots & \ddots & \ddots & 0 \\ 0 & \cdots & 0 & 0 & 1 \\ 1 & 0 & \cdots & 0 & 0 \end{bmatrix}, \tag{4.3}$$

we express the Hamiltonian as

$$\begin{aligned} \mathcal{H}_s^{\mathrm{HF}}(t) &= \mathrm{diag}\left[\mathcal{P}_{1,s}(t), \ldots, \mathcal{P}_{N,s}(t)\right] \\ &\quad + U^{\dagger}\mathrm{diag}\left[\mathcal{Q}_{1,s}(t), \ldots, \mathcal{Q}_{N,s}(t)\right] U, \end{aligned} \tag{4.4}$$

where the 2×2 matrices

$$\mathcal{P}_{n,s}(t) = \begin{bmatrix} -\frac{\beta}{2}[v_n(t) - u_{n-1}(t)] \\ \quad + \frac{U_{\mathrm{M}}}{2} A_{n,-s}(t) \\ \quad + \frac{V_{\mathrm{MM}}}{2} B_n(t) \\ \quad + \frac{V_{\mathrm{MXM}}}{2} B_{n-1}(t) \end{bmatrix} \quad \begin{bmatrix} -t_{\mathrm{MM}} - V_{\mathrm{MM}} P_{n,s}(t) \end{bmatrix}$$

$$\begin{bmatrix} -t_{\mathrm{MM}} - V_{\mathrm{MM}} P^*_{n,s}(t) \end{bmatrix} \quad \begin{bmatrix} -\frac{\beta}{2}[u_n(t) - v_n(t)] \\ \quad + \frac{U_{\mathrm{M}}}{2} B_{n,-s}(t) \\ \quad + \frac{V_{\mathrm{MM}}}{2} A_n(t) \\ \quad + \frac{V_{\mathrm{MXM}}}{2} A_{n+1}(t) \end{bmatrix},$$

$$\mathcal{Q}_{n,s}(t) = \begin{bmatrix} -\frac{\beta}{2}[u_n(t) - v_n(t)] \\ \quad + \frac{U_{\mathrm{M}}}{2} B_{n,-s}(t) \\ \quad + \frac{V_{\mathrm{MM}}}{2} A_n(t) \\ \quad + \frac{V_{\mathrm{MXM}}}{2} A_{n+1}(t) \end{bmatrix} \quad \begin{bmatrix} -t_{\mathrm{MXM}} \\ +\alpha[v_{n+1}(t) - v_n(t)] \\ -V_{\mathrm{MXM}} Q_{n,s}(t) \end{bmatrix}$$

$$\begin{bmatrix} -t_{\mathrm{MXM}} \\ +\alpha[v_{n+1}(t) - v_n(t)] \\ -V_{\mathrm{MXM}} Q^*_{n,s}(t) \end{bmatrix} \quad \begin{bmatrix} -\frac{\beta}{2}[v_{n+1}(t) - u_n(t)] \\ \quad + \frac{U_{\mathrm{M}}}{2} A_{n+1,-s}(t) \\ \quad + \frac{V_{\mathrm{MM}}}{2} B_{n+1}(t) \\ \quad + \frac{V_{\mathrm{MXM}}}{2} B_n(t) \end{bmatrix} \tag{4.5}$$

are self-consistently calculated through

$$\begin{aligned} A_n(t) &= \sum_s A_{n,s}(t) = \sum_s {\sum_{\mu}}' \left|\vartheta_{\mu,n,s}(t)\right|^2, \\ B_n(t) &= \sum_s B_{n,s}(t) = \sum_s {\sum_{\mu}}' \left|\varphi_{\mu,n,s}(t)\right|^2, \\ P_n(t) &= \sum_s P_{n,s}(t) = \sum_s {\sum_{\mu}}' \vartheta^*_{\mu,n,s}(t)\varphi_{\mu,n,s}(t), \\ Q_n(t) &= \sum_s Q_{n,s}(t) = \sum_s {\sum_{\mu}}' \varphi^*_{\mu,n,s}(t)\vartheta_{\mu,n+1,s}(t), \end{aligned} \tag{4.6}$$

with $\sum'$ denoting the summation over the initially occupied levels. Now the HF wavevector $\{\vartheta_{\mu,n,s}, \varphi_{\mu,n,s}\}$ and the lattice configuration $\{u_n, v_n\}$ are both time-dependent. Discretizing the time variable as $t_j = j\Delta t$ ($j = 0, 1, 2, \ldots$) with the interval Δt much smaller than $\omega_{\mathrm{eff}}^{-1} \equiv \sqrt{M_{\mathrm{M}} M_{\mathrm{X}}/(2M_{\mathrm{M}} + M_{\mathrm{X}})K_{\mathrm{MX}}}$, we schematically integrate equation (4.1):

$$\Psi_{\mu,s}(t_{j+1}) = \hat{T}\exp\left[-\frac{\mathrm{i}}{\hbar}\int_{t_j}^{t_j+\Delta t} \mathcal{H}_s^{\mathrm{HF}}(t)\,\mathrm{d}t\right]\Psi_{\mu,s}(t_j), \tag{4.7}$$

where $\hat{T}$ denotes the time ordering. Employing a general decomposition theory of ordered exponentials [48], together with the expression (4.4), we can carry out the time evolution of equation (4.7) without numerically diagonalizing $\mathcal{H}_s^{\mathrm{HF}}(t)$ at every time step [49], which serves to accelerate the calculation. We adopt a fractal decomposition up to the third order of Δt [50, 51].

The lattice dynamics is governed by Newton's equation of motion:

$$\begin{aligned} M_{\mathrm{X}}\ddot{u}_n(t) &= K_{\mathrm{MX}}[v_{n+1}(t) - 2u_n(t) + v_n(t)] \\ &\quad - \beta[A_{n+1}(t) - B_n(t)] \equiv F_n(t), \\ 2M_{\mathrm{M}}\ddot{v}_n(t) &= K_{\mathrm{MX}}[u_n(t) - 2v_n(t) + u_{n-1}(t)] \\ &\quad + \beta[A_n(t) - B_n(t)] + \alpha[Q_n(t) + Q^*_n(t) \\ &\quad - Q_{n-1}(t) - Q^*_{n-1}(t)] \equiv G_n(t). \end{aligned} \tag{4.8}$$

With the discrete time variable, we evolve the lattice configuration as

$$\begin{aligned} u_n(t_{j+1}) &= u_n(t_j) + \dot{u}_n(t_j)\Delta t, \\ \dot{u}_n(t_{j+1}) &= \dot{u}_n(t_j) + \frac{F_n(t_j)}{M_{\mathrm{X}}}\Delta t, \\ v_n(t_{j+1}) &= v_n(t_j) + \dot{v}_n(t_j)\Delta t, \\ \dot{v}_n(t_{j+1}) &= \dot{v}_n(t_j) + \frac{G_n(t_j)}{2M_{\mathrm{M}}}\Delta t. \end{aligned} \tag{4.9}$$

We start any calculation from a stationary lattice of the CDW or ACP type:

$$\begin{aligned} v_n(t_0) - u_{n-1}(t_0) &= \sigma(-1)^n\lambda + \Delta l_n(t_0), \\ u_n(t_0) - v_n(t_0) &= (-1)^n\lambda + \Delta r_n(t_0), \end{aligned} \tag{4.10}$$

$$\dot{u}_n(t_0) = \dot{v}_n(t_0) = 0, \tag{4.11}$$

where $\Delta l_n(t_0), \Delta r_n(t_0)(\ll\lambda)$ are introduced at random as thermal fluctuations.

In an attempt to guide future experiments, we adopt a realistic set of parameters: $t_{\mathrm{MXM}} = 1.5$ eV, $K_{\mathrm{MX}} = 8.0$ eV Å^{-2}, $2M_{\mathrm{M}} = 13.4 \times 10^5\, M_{\mathrm{e}}$ and $M_{\mathrm{X}} = 2.3 \times 10^5\, M_{\mathrm{e}}$ [35, 36], where M_{e} is the electron mass. Numerical integration is reliable enough with $\Delta t = 10^{-3}\omega_{\mathrm{eff}}^{-1} = 0.0255$ fs. The initial disorder $(\Delta l_n(t_0), \Delta r_n(t_0))$ is restricted to $10^{-4}\lambda$, which corresponds to low temperatures of 10 K $\lesssim T \simeq 0.05\hbar\omega_{\mathrm{eff}}/k_{\mathrm{B}} \lesssim 20$ K, where both CDW and ACP ground states are fully stabilized [13, 21].

We first pump up an electron to the first excited state and observe the following time evolution. Typical examples are shown in figures 3 and 4. Photoproduction of neutral (1) and charged (2) soliton–antisoliton pairs and their geminate recombination in the early stage (3) are clearly found on both

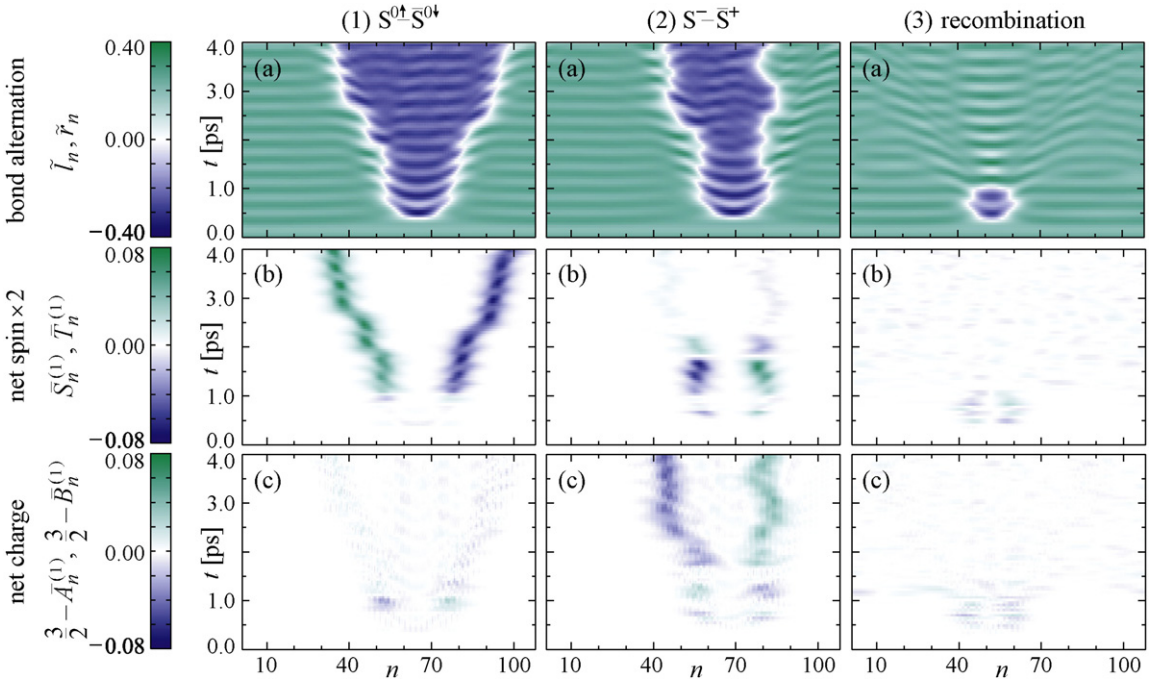

Figure 3. Contour plots of bond, spin and charge variables as functions of space and time for the first excited state of a Pt_2X chain with a CDW ($\sigma = 1$) background: (a) the bond order parameters $\tilde{l}_n(t) = \sigma(-1)^n[-l_{n-1}(t) + 2l_n(t) - l_{n+1}(t)]/4$, $\tilde{r}_n(t) = (-1)^n[-r_{n-1}(t) + 2r_n(t) - r_{n+1}(t)]/4$; (b) twice the net spin densities $\bar{S}_n^{(1)}(t) = \sum_s s\bar{A}_{n,s}^{(1)}(t) = \sum_s s[A_{n-1,s}^{(1)}(t) + 2A_{n,s}^{(1)}(t) + A_{n+1,s}^{(1)}(t)]/4$, $\bar{T}_n^{(1)}(t) = \sum_s s\bar{B}_{n,s}^{(1)}(t) = \sum_s s[B_{n-1,s}^{(1)}(t) + 2B_{n,s}^{(1)}(t) + B_{n+1,s}^{(1)}(t)]/4$; (c) the net electron densities $\bar{A}_n^{(1)}(t) = \sum_s \bar{A}_{n,s}^{(1)}(t)$, $\bar{B}_n^{(1)}(t) = \sum_s \bar{B}_{n,s}^{(1)}(t)$; where $l_n(t) = v_n(t) - u_{n-1}(t)$ and $r_n(t) = u_n(t) - v_n(t)$, while $A_{n,s}^{(l)}(t) = \sum_\mu f_{\mu,s}^{(l)}|\vartheta_{\mu,n,s}(t)|^2$ and $B_{n,s}^{(l)}(t) = \sum_\mu f_{\mu,s}^{(l)}|\varphi_{\mu,n,s}(t)|^2$ with $f_{\mu,s}^{(l)}$ being the time-independent distribution function of spin-s electrons for the lth excited state. When $l = 1$, $f_{\mu,s}^{(l)} = 1$ for $\mu \leqslant 3N/2$ and $f_{\mu,s}^{(l)} = 0$ for $\mu > 3N/2$ but $f_{3N/2,\uparrow}^{(l)} = 0$ and $f_{3N/2+1,\uparrow}^{(l)} = 1$.

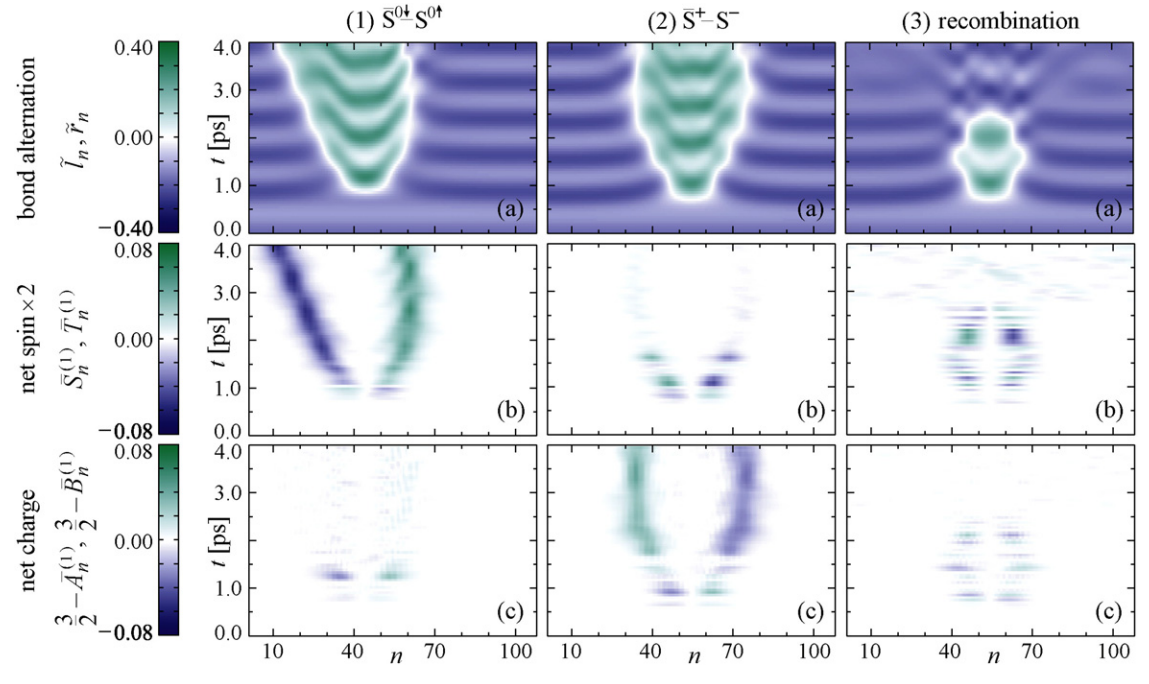

Figure 4. The same as figure 3 but with an ACP ($\sigma = -1$) background.

CDW and ACP backgrounds, supporting the analytical findings in figure 2. In all the cases, a single and local defect is first nucleated on the ground-state lattice configuration and further lattice relaxation induces excess spin or charge density in the defect centres. Although the photoexcitations are finalized into $S^{0\uparrow} - \bar{S}^{0\downarrow}$ and $S^{-} - \bar{S}^{+}$ pairs along paths 1 and 2, respectively,

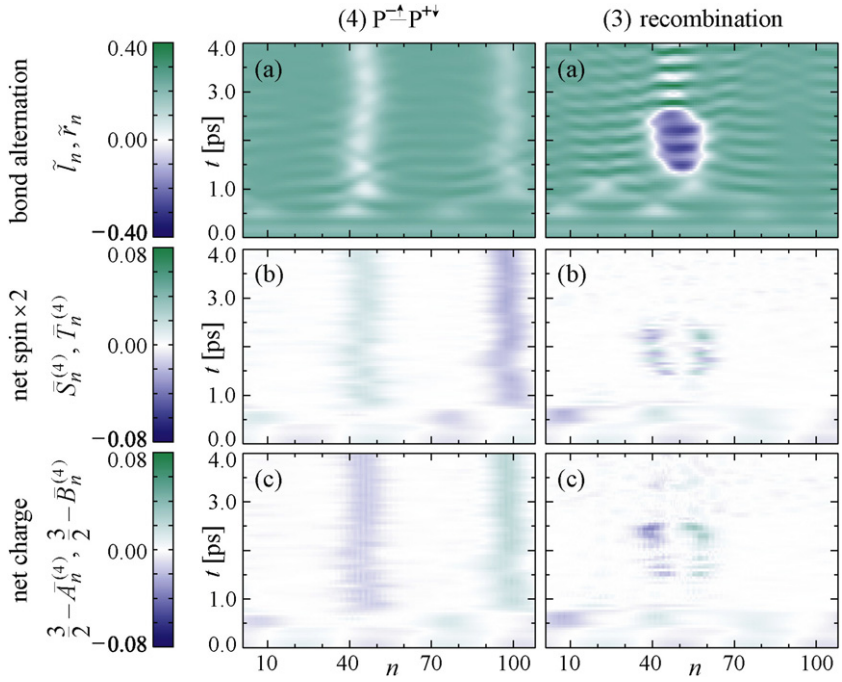

Figure 5. The same as figure 3 but for the fourth excited state. When $l = 4$, $f^{(l)}_{\mu,s} = 1$ for $\mu \leqslant 3N/2$ and $f^{(l)}_{\mu,s} = 0$ for $\mu > 3N/2$ but $f^{(l)}_{3N/2-1,\uparrow} = 0$ and $f^{(l)}_{3N/2+2,\uparrow} = 1$.

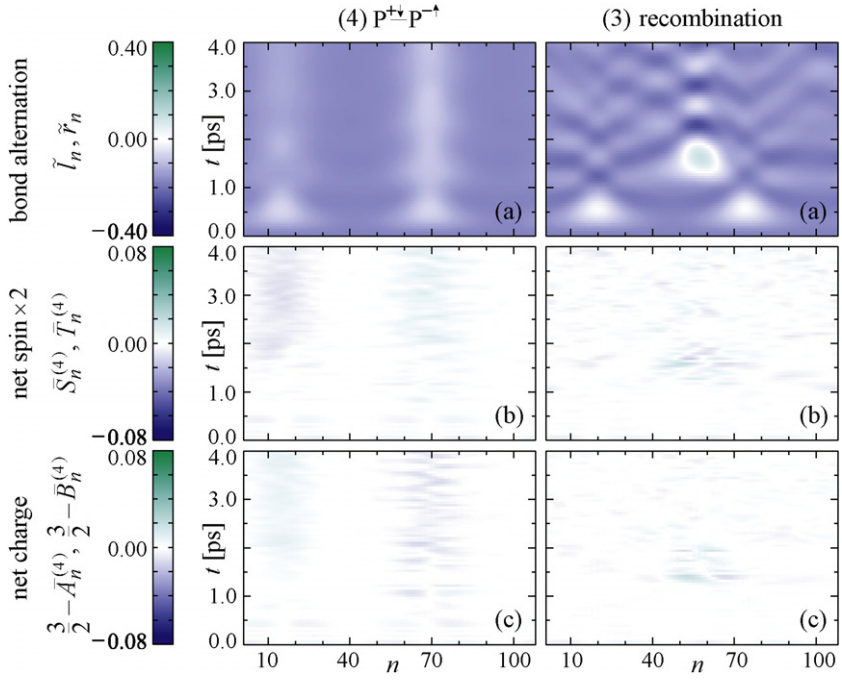

Figure 6. The same as figure 5 but with an ACP ($\sigma = -1$) background.

the early kinks on path 2 convey net spins rather than charges and then even wear charges and spins alternately. This is strong evidence for tunnelling between the energy surfaces E_1 and E_0 in figure 2. Kinks seem to be more frequently stabilized into spin solitons than into charged ones at low temperatures (see figure 7 later on). The oscillation between neutral and charged kinks is generally observed on the occasion of their geminate recombinations.

The CDW and ACP backgrounds oscillate at regular intervals but with different frequencies. The CDW oscillation is mainly caused by the halogen sublattice, while the ACP oscillation is by the platinum sublattice. The ratio of the former frequency to the latter one is indeed $\sqrt{2M_{\mathrm{M}}/M_{\mathrm{X}}} \simeq 2.4$. Figures 3(3) and 4(3) demonstrate in common that a newborn soliton–antisoliton pair survives twice the oscillational period

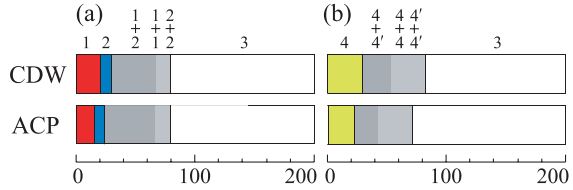

Figure 7. Characterization of photoproducts at the moment of four picoseconds after pumping up an electron to the first (a) and fourth (b) excited states with CDW and ACP backgrounds. Every case we observe two hundred samples changing the initial condition at random and encounter neutral soliton–antisoliton pairs (1), charged soliton–antisoliton pairs (2), linear combinations of them, which result in kink–antikink pairs with excess spin and charge densities of fraction $(1+2)$ and those without any excess density of spin and charge $(1+1, 2+2)$, polaron pairs $(4, 4')$, linear combinations of them, which result in pairs of dips on the bond order parameters with either spin or charge excess density $(4+4')$ and those without any excess density of spin and charge $(4+4, 4'+4')$, and no local defect detectable (3). The categorization is compactly summarized in table 1.

Table 1. Classification of photoproducts.

Character	Configuration	Label
Neutral soliton	$S^{0\uparrow}-\bar{S}^{0\downarrow}$, $S^{0\downarrow}-\bar{S}^{0\uparrow}$	1
Charged soliton	$S^{+}-\bar{S}^{-}$, $S^{-}-\bar{S}^{+}$	2
Kink with fractional spin and charge	$K^{\frac{+\uparrow}{2}}-\bar{K}^{\frac{-\downarrow}{2}}$, $K^{\frac{-\downarrow}{2}}-\bar{K}^{\frac{+\uparrow}{2}}$ $K^{\frac{-\uparrow}{2}}-\bar{K}^{\frac{+\downarrow}{2}}$, $K^{\frac{+\downarrow}{2}}-\bar{K}^{\frac{-\uparrow}{2}}$	$1+2$
Kink with neither spin nor charge	$K-\bar{K}$	$1+1$ $2+2$
Polaron	$P^{-\uparrow}-P^{+\downarrow}$, $P^{+\downarrow}-P^{-\uparrow}$	4
	$P^{-\downarrow}-P^{+\uparrow}$, $P^{+\uparrow}-P^{-\downarrow}$	$4'$
Dip with either spin or charge	$D^{\uparrow}-D^{\downarrow}$, $D^{\downarrow}-D^{\uparrow}$ $D^{+}-D^{-}$, $D^{-}-D^{+}$	$4+4'$
Dip with neither spin nor charge	$D-D$	$4+4$ $4'+4'$

and then recombines to disappear. ACP solitons are consequently longer-lived than CDW solitons.

Next we pump up an electron to the fourth excited state. Typical examples are shown in figures 5 and 6. Now far distant defects in a pair, accompanied by excess spin and charge densities all along, suddenly appear within much less than picoseconds, which is again consistent with the analytical findings in figure 2. Any defect is more delocalized on an ACP background than on a CDW background and polarons are less localized than solitons in general. The excess spin and charge densities accompanying the ACP polarons are widely distributed. All the findings accord with the preceding variational calculations. When the interdefect distance d is much larger than the defect width ξ, the solitonic and polaronic wavefunctions (3.1) and (3.2) are optimized at $\xi = 3.45$ and $\xi = 5.94$, respectively, in the case of a CDW background, whereas they are most stable at $\xi = 4.25$ and $\xi = 8.00$, respectively, in the case of an ACP background. The smaller gap, the wider extent of any defect. The adopted CDW and ACP ground states possess Peierls gaps of 0.68 eV and 0.53 eV, respectively. The gap, unless too large, well scales the defect extent [36]. The asymmetric lattice deformation of a pair of far distant polarons was found in PtX chains as well [33]. A pair of polarons often recombine, failing to stably separate away from each other, where they disappear necessarily via an STE. Unless the STE is luminescent, it nonradiatively relaxes further into a solitonic state, as we have already observed in figures 3 and 4. Thus higher-energy excitations are longer-lived in general.

We close our time-dependent HF calculation estimating how probable each photoproduct is. We carry out numerical integrations with varying initial condition and count in figure 7 the resultant photoproducts classified into several categories. High-energy excitations above the electron–hole continuum tend to relax into polarons, while excitons pumped within the optical gap are self-localized and then dissociated into solitons and antisolitons in pairs. Solitons are easier neutral than charged. Both solitons and polarons are so fragile that the major part of them disappears in pairs within a few picoseconds. There appear kinks and dips on the bond order parameters with unusual spin and/or charge densities in their centres, which can be regarded as linear combinations of prototypical solitons and polarons [52]. A pair of kinks and antikinks wearing half of the full electron/hole charge and spin, $K^{\frac{+\uparrow}{2}}-\bar{K}^{\frac{-\downarrow}{2}}$, for example, consists of $S^{0\uparrow}-\bar{S}^{0\downarrow}$ and $S^{+}-\bar{S}^{-}$ in phase and of equal weight. Such resonant states are better understandable if we observe figures 3 and 4 in more detail. When a pair of kinks and antikinks separate away from each other or recombine to disappear, not only do excess spin and charge densities alternate, but even their signs are oscillating, in the centres of them. Such striking fluctuations of spin and/or charge densities are characteristic of photoproducts decaying nonradiatively rather than by luminescence.

5. Summary and discussion

Coexistent neutral and charged solitons as stable photoproducts are characteristic of Pt_2X chains. Mononuclear platinum complexes should be described with larger Coulomb interactions, where neutral solitons are probable photoproducts, while charged solitons are much less expected due to an energy barrier on the way from an STE to them in a pair, as is shown in figure 8. Conversion of photoinduced charge-transfer excitons into neutral soliton pairs has been indeed detected in the chloro and bromo complexes, $[Pt(en)_2Cl](ClO_4)_2$ and $[Pt(en)_2Br](ClO_4)_2$ [39, 53–55]. The photoinduced valence anomalies are all ESR-active and a comparative study of the heterometal compound $[Pt(en)_2][Pd(en)_2Br_2](ClO_4)_4$, whose ground state is no longer degenerate, enables us to distinguish spin solitons from polarons.

No doubt the simultaneous stabilization of neutral and charged solitons against STEs is attributable to the reduction of Coulomb interactions, but they owe much to the binuclear unit-assembled structure as well. When we artificially model PtX chains with a similar set of correlation and coupling parameters as adopted in the present Pt_2X chains, charged solitons indeed look available from STEs, but neutral solitons turn hardly reachable instead, as is shown in figure 9. Such a situation more or less agrees with experimental findings in Pt–I chains. There is a report [42, 43] that photocarriers in $[Pt(en)_2I](ClO_4)_2$ may be charged solitons. Since the halogen

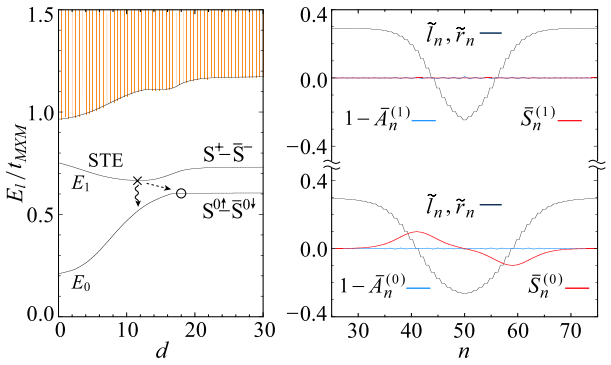

Figure 8. The solitonic relaxation channel of a photoexcited PtX chain whose ground state is of the CDW type, where $U_M/t_{MXM} = 0.9$, $V_{MXM}/t_{MXM} = 0.35$ and $\beta/\sqrt{t_{MXM}K_{MX}} = 0.7$. Electronic structures of the lowest- and second-lowest-lying states, together with their background lattice configurations, are snapshotted at $d = 18$ (○) and $d = 12$ (×), respectively.

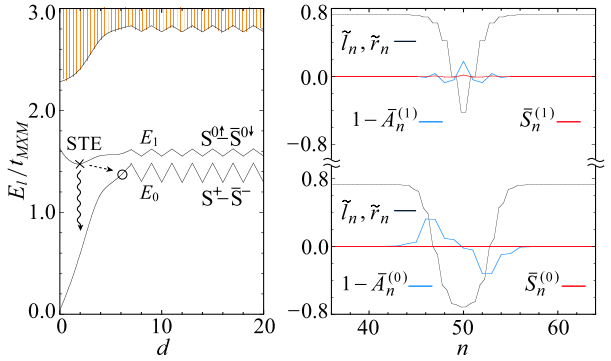

Figure 9. The same as figure 8 but $U_M/t_{MXM} = 0.5$, $V_{MXM}/t_{MXM} = 0.05$ and $\beta/\sqrt{t_{MXM}K_{MX}} = 1.0$. Snapshots are taken at $d = 2$ (○) and $d = 6$ (×).

character increases in the platinum wavefunctions in the order Cl < Br < I, the d–p transfers are enhanced and the Coulomb interactions are therefore suppressed effectively in the iodo complexes. The stabilization of charged solitons instead of neutral ones is thus understandable. The generated charged solitons are rather long-lived, possibly tunnelling through a bumpy potential [43].

The room-temperature conductivity of $Pt_2(dta)_4I$ is about nine orders of magnitude higher than those of typical PtX complexes [21]. Photocarriers must be highly mobile in Pt_2X chains. Spin solitons, charged solitons and polarons are likely to come together on such a fascinating stage. The real-time simulation reveals quantum tunnelling between neutral and charged solitons, breathing motion of charged solitons in a pair, and asymmetry between electron and hole polarons, which are all stimulative toward further experiments.

The band filling of the dta family $M_2(RCS_2)_4I$ (M = Pt, Ni; R = C_nH_{2n+1}) [3, 4, 27, 28] might be varied in general because of their neutral chain structure. Under doping, bipolarons [5, 6, 56–58], that is, doubly charged bound polarons, also come into our interest. Besides Pt_2X chains, ladder-shaped PtX complexes have been recently synthesized, [59, 60] exhibiting ground-state variations [61–63]. We hope our calculations will stimulate extensive optical explorations of new varieties of metal–halide complexes.

Acknowledgments

The authors thank S Kuroda and K Iwano for fruitful discussions. This work was supported by the Ministry of Education, Culture, Sports, Science, and Technology of Japan.

References

[1] Che C-M, Herbstein F H, Schaefer W P, Marsh R E and Gray H B 1983 *J. Am. Chem. Soc.* **105** 4604
[2] Clark R J H, Kurmoo M, Dawes H M and Hursthouse M B 1986 *Inorg. Chem.* **25** 409
[3] Bellitto C, Flamini A, Gastaldi L and Scaramuzza L 1983 *Inorg. Chem.* **22** 444
[4] Bellitto C, Dessy G and Fares V 1985 *Inorg. Chem.* **24** 2815
[5] Gammel J T, Saxena A, Batistić I, Bishop A R and Phillpot S R 1992 *Phys. Rev.* B **45** 6408
[6] Weber-Milbrodt S W, Gammel J T, Bishop A R and Loh E Y Jr 1992 *Phys. Rev.* B **45** 6435
[7] Yamamoto S 2001 *Phys. Rev.* B **63** 125124
[8] Kuwabara M and Yonemitsu K 2001 *J. Mater. Chem.* **11** 2163
[9] Butler L G, Zietlow M H, Che C-M, Schaefer W P, Sridhar S, Grunthaner P J, Swanson B I, Clark R J H and Gray H B 1988 *J. Am. Chem. Soc.* **110** 1155
[10] Kimura N, Ohki H, Ikeda R and Yamashita M 1994 *Chem. Phys. Lett.* **220** 40
[11] Yamashita M, Miya S, Kawashima T, Manabe T, Sonoyama T, Kitagawa H, Mitani T, Okamoto H and Ikeda R 1999 *J. Am. Chem. Soc.* **121** 2321
[12] Yamamoto S 2000 *J. Phys. Soc. Japan* **69** 13
[13] Swanson B I, Stroud M A, Conradson S D and Zietlow M H 1988 *Solid State Commun.* **65** 1405
[14] Kanner G S, Gammel J T, Love S P, Johnson S R, Scott B and Swanson B I 1994 *Phys. Rev.* B **50** R18682
[15] Yamamoto S 2001 *Phys. Rev.* B **64** 140102(R)
[16] Yamamoto S 2002 *J. Phys. Chem. Solids* **63** 1489
[17] Matsuzaki H, Matsuoka T, Kishida H, Takizawa K, Miyasaka H, Sugiura K, Yamashita M and Okamoto H 2003 *Phys. Rev. Lett.* **90** 046401
[18] Yonemitsu K and Miyashita N 2003 *Phys. Rev.* B **68** 075113
[19] Kitagawa H, Onodera N, Ahn J-S, Mitani T, Toriumi K and Yamashita M 1997 *Synth. Met.* **86** 1931
[20] Calzolari A, Alexandre S S, Zamora F and Felice R D 2008 *J. Am. Chem. Soc.* **130** 5552
[21] Kitagawa H, Onodera N, Sonoyama T, Yamamoto M, Fukawa T, Mitani T, Seto M and Maeda Y 1999 *J. Am. Chem. Soc.* **121** 10068
[22] Yamamoto S 2001 *J. Phys. Soc. Japan* **70** 1198
[23] Ikeuchi S, Saito K, Nakazawa Y, Sato A, Mitsumi M, Toriumi K and Sorai M 2002 *Phys. Rev.* B **66** 115110
[24] Ikeuchi S, Saito K, Nakazawa Y, Mitsumi M, Toriumi K and Sorai M 2004 *J. Phys. Chem.* B **108** 387
[25] Borshch S A, Prassides K, Robert V and Solonenko A O 1998 *J. Chem. Phys.* **109** 4562
[26] Wakabayashi Y, Kobayashi A, Sawa H, Ohsumi H, Ikeda N and Kitagawa H 2006 *J. Am. Chem. Soc.* **128** 6676
[27] Mitsumi M, Murase T, Kishida H, Yoshinari T, Ozawa Y, Toriumi K, Sonoyama T, Kitagawa H and Mitani T 2001 *J. Am. Chem. Soc.* **123** 11179
[28] Mitsumi M, Kitamura K, Morinaga A, Ozawa Y, Kobayashi M, Toriumi K, Iso Y, Kitagawa H and Mitani T 2002 *Angew. Chem. Int. Edn* **41** 2767
[29] Ichinose S 1984 *Solid State Commun.* **50** 137
[30] Onodera Y 1987 *J. Phys. Soc. Japan* **56** 250

[31] Baeriswyl D and Bishop A R 1988 *J. Phys. C: Solid State Phys.* **21** 339
[32] Mishima A and Nasu K 1989 *Phys. Rev.* B **39** 5758
[33] Mishima A and Nasu K 1989 *Phys. Rev.* B **39** 5763
[34] Gammel J T, Donohoe R J, Bishop A R and Swanson B I 1990 *Phys. Rev.* B **42** 10566
[35] Yamamoto S and Ichioka M 2002 *J. Phys. Soc. Japan* **71** 189
[36] Yamamoto S 2002 *Phys. Rev.* B **66** 165113
[37] Conradson S D, Stroud M A, Zietlow M H, Swanson B I, Baeriswyl D and Bishop A R 1988 *Solid State Commun.* **65** 723
[38] Tanaka H, Kuroda S, Yamashita T, Mitsumi M and Toriumi K 2003 *J. Phys. Soc. Japan* **72** 2169
[39] Sakai M, Kuroda N and Nishina Y 1989 *Phys. Rev.* B **40** 3066
[40] Kurita S, Haruki M and Miyagawa K 1988 *J. Phys. Soc. Japan* **57** 1789
[41] Donohoe R J, Ekberg S A, Tait C D and Swanson B I 1989 *Solid State Commun.* **71** 49
[42] Okamoto H, Mitani T, Toriumi K and Yamashita M 1992 *Phys. Rev. Lett.* **69** 2248
[43] Okamoto H, Oka Y, Mitani T and Yamashita M 1997 *Phys. Rev.* B **55** 6330
[44] Iwano K 1997 *J. Phys. Soc. Japan* **66** 1088
[45] Ohara J and Yamamoto S 2006 *Phys. Rev.* B **73** 045122
[46] Saxena A, Shuai Z, Gammel J T, Batistić I, Alouani M, Brédas J L and Bishop A R 1995 *Synth. Met.* **71** 1659
[47] Ohara J and Yamamoto S 2005 *J. Phys. Chem. Solids* **66** 1571
[48] Suzuki M 1992 *Phys. Lett.* A **165** 387
[49] Kinoshita M, Hirano Y, Kuwabara M and Ono Y 1997 *J. Phys. Soc. Japan* **66** 703
[50] Suzuki M 1993 *Proc. Japan Acad.* B **69** 161
[51] Terai A and Ono Y 1993 *Prog. Theor. Phys. Suppl.* **113** 177
[52] Hirano Y and Ono Y 1998 *J. Phys. Soc. Japan* **67** 3835
Hirano Y and Ono Y 2000 *J. Phys. Soc. Japan* **69** 2131
[53] Sakai M, Kuroda N, Suezawa M, Nishina Y, Sumino K and Yamashita M 1992 *J. Phys. Soc. Japan* **61** 1326
[54] Kuroda N, Ito M, Nishina Y, Kawamori A, Kodera Y and Matsukawa T 1993 *Phys. Rev.* B **48** 4245
[55] Okamoto H, Kaga Y, Shimada Y, Oka Y, Iwasa Y, Mitani T and Yamashita M 1998 *Phys. Rev. Lett.* **80** 861
[56] Haruki M and Kurita S 1989 *Phys. Rev.* B **39** 5706
[57] Mishima A and Nasu K 1989 *Phys. Rev.* B **40** 5593
[58] Batistić I, Huang X Z, Bishop A R and Saxena A 1993 *Phys. Rev.* B **48** 6065
[59] Kobayashi A and Kitagawa H 2006 *J. Am. Chem. Soc.* **128** 12066
[60] Kawakami D, Yamashita M, Matsunaga S, Takaishi S, Kajiwara T, Miyasaka H, Sugiura K, Matsuzaki H and Okamoto H 2006 *Angew. Chem.* **118** 7372
[61] Funase K and Yamamoto S 2006 *J. Phys. Soc. Japan* **75** 044717
[62] Iwano K and Shimoi Y 2007 *J. Phys. Soc. Japan* **76** 063708
[63] Yamamoto S and Ohara J 2007 *Phys. Rev.* B **76** 235116